Supplemental Material for Magnetic resonance detection of individual proton spins using quantum reporters

A. O. Sushkov,[1,2] I. Lovchinsky,[1] N. Chisholm,[3] R. L. Walsworth,[1,4,5] H. Park,[1,2,6,*] and M. D. Lukin[1,†]

[1] *Department of Physics, Harvard University, Cambridge, MA 02138, USA*
[2] *Department of Chemistry and Chemical Biology, Harvard University, Cambridge, MA 02138, USA*
[3] *School of Engineering and Applied Sciences, Harvard University, Cambridge, MA 02138, USA*
[4] *Harvard-Smithsonian Center for Astrophysics, Cambridge, Massachusetts 02138, USA*
[5] *Center for Brain Science, Harvard University, Cambridge, Massachusetts 02138, USA*
[6] *Broad Institute of MIT and Harvard, 7 Cambridge Center, Cambridge, MA, 02142, USA*

I. MATERIALS AND MEASUREMENT APPARATUS

A. Diamond sample

The sample used in this work is a polished, single-crystal electronic grade diamond grown by chemical vapor deposition (Element Six), containing substitutional nitrogen and boron in concentrations less than 5 parts per billion (ppb) and 1 ppb respectively. Prior to implantation, the {100} diamond surface was etched approximately 2 μm, using an Ar-Cl_2 plasma etch (25 sccm Ar, 40 sccm Cl_2, ICP RF 400 W, bias RF 250 W, duration 150 s), followed by an O_2 plasma etch (30 sccm O_2, ICP RF 700 W, bias RF 100 W, duration 150 s). Nitrogen implantation was done by INNOViON Corporation using a $^{15}N^+$ dosage of 10^9 cm^{-2} and an implantation energy of 2.5 keV. The implanted diamond was annealed in vacuum using the following procedure: (a) 6 hour ramp to 400°C, (b) 6 hours at 400°C, (c) 6 hour ramp to 800°C, (d) 8 hours at 800°C and (e) 6 hour ramp to room temperature. After annealing, the diamond was cleaned in a 3-acid mixture (equal volumes of concentrated H_2SO_4, HNO_3, and $HClO_4$) for two hours under reflux conditions. The same cleaning procedure was used to re-set the locations of the reporter spins on the diamond surface.

B. Optical setup

A home-built scanning confocal microscope was used to optically address and read out single NV centers. An RF transmission line was fabricated on the surface of a glass coverslip, and the diamond was placed NV-side down on top of this coverslip. The inverted Nikon Plan Fluor 100x oil immersion objective (NA = 1.3) was positioned under the coverslip. Its vertical position was controlled with a piezoelectric scanner (Physik Instrumente P-721 PIFOC) and the lateral position of the laser beam focus was controlled with a closed-loop scanning galvanometer (Thorlabs GVS012). Optical excitation was performed with a 532 nm laser (Information Unlimited, MLLIII532-200-1) modulated with an acousto-optic modulator (Isomet Corporation, 1250C-974) in a double-pass configuration. NV center fluorescence was filtered with a 532 nm notch filter (Semrock, NF03-532E) and a 633 nm long-pass filter (Semorck, LP02-633RU) and collected using a single-photon counting module (PerkinElmer, SPCM-AQRH-14-FC). The acousto-optic modulator and the single-photon counting module were gated using TTL pulses produced by a 500 MHz PulseBlasterESR-PRO pulse generator from Spincore Technologies. Typical NV center fluorescence count rate was 20 kHz, and photon counter acquisition window for each sequence repetition was 500 ns.

C. RF setup

The RF tones, used to address the NV centers and the surface reporter spins, were generated by two Stanford Research SG384 signal generators. The IQ modulation inputs were used to control the x and y quadrature amplitudes of the generator that addressed the NV center. The RF pulses in each channel were generated by the switches (MiniCircuits ZASWA-2-50DR+), controlled by the TTL pulses from the PulseBlasterESR-PRO, and power boosted by an amplifier (three amplifiers were used, depending on the frequency: MiniCircuits ZHL-20W-13+, ZHL-30W-252-S+, and ZHL-16W-43-S+). The two RF channels were combined using an MCLI PS2-109 power splitter, and coupled into the 50 Ω-terminated RF transmission line with the diamond sample on top.

II. NV CENTERS AND DEPTH MEASUREMENTS

The DEER experiments were performed on a total of 16 NV centers. 12/16 showed clear DEER collapse due to reporter spins, on the time scale shorter than their $T_2^{(nv)}$, 2/16 showed DEER collapse on the order of $T_2^{(nv)}$, and 2/16 showed no DEER collapse. NVs A and B were selected for their fastest DEER collapse, which likely means they are among the most shallow of the NV centers. Reporter sequence experiments were performed only with NVs A and B.

The depths of each of these two NV centers were determined by covering the diamond surface with immersion oil, and measuring the amplitude of the magnetic field created at the location of the NV center by the immersion oil proton magnetic moments, precessing at the Larmor frequency. The dynamical decoupling XY-k sequence was used to perform this ac magnetometry experiment, see data shown in Fig. S1. The details of the measurement and fitting procedure are described in a manuscript in preparation[1]. This method yielded the following depths: NV A $\rightarrow (3.3 \pm 0.2)$ nm, and NV B $\rightarrow (3.6 \pm 0.3)$ nm.

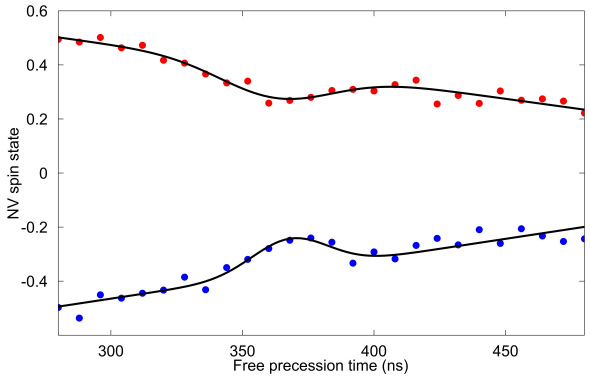

FIG. S1: The results of dynamical decoupling experiment (XY-16 pulse sequence) on NV A, from which we extract its depth.

When a separate diamond sample, with an unpolished surface, implanted and annealed with the same parameters as the one used in our work, was treated at 465°C in an O_2 atmosphere[2], we found that the DEER signals were absent for 11 out of the 12 NV centers for which measurements were taken, and one NV center showed a "weak" DEER signal with the DEER collapse on the order of NV decoherence time $T_2^{(nv)}$. We concluded that this treatment removed the reporter spins from the diamond surface.

III. LOCALIZING REPORTER SPINS ON THE DIAMOND SURFACE

A. The double electron-electron resonance experiment

The strength of the magnetic dipole coupling between the NV center and the surface spin network was characterized using the double electron-electron resonance (DEER) pulse sequence.

The dipole-dipole interaction Hamiltonian between the NV center spin $\boldsymbol{S}$ and the surface reporter spin $\boldsymbol{J}$ is:

$$H_d = \frac{\hbar^2\gamma_e^2}{r_s^3}\left[\boldsymbol{S}\cdot\boldsymbol{J} - 3\frac{(\boldsymbol{S}\cdot\boldsymbol{r}_s)(\boldsymbol{J}\cdot\boldsymbol{r}_s)}{r_s^2}\right], \tag{1}$$

where $\boldsymbol{r}_s$ is the vector from the NV center to the reporter spin. When the magnetic field B is aligned with the NV center axis, we can neglect all non-secular terms, and consider only the terms that commute with S_z and J_z:

$$H_d = \frac{\hbar^2\gamma_e^2}{r_s^3}\left(1 - 3\cos^2\theta_s\right) S_z J_z = \hbar k_s S_z J_z, \tag{2}$$

where θ_s is the angle that vector $\boldsymbol{r}_s$ makes with the magnetic field, and the coupling strength is

$$k_s = \frac{\hbar\gamma_e^2}{r_s^3}\left(1 - 3\cos^2\theta_s\right). \tag{3}$$

The NV center $|m_s = 0\rangle$ state population after the DEER sequence with duration t_{nv} is given by

$$S = \frac{1}{2}\left[1 + \cos(k_s J_z t_{nv})\right] = \frac{1}{2}\left[1 + \cos(k_s \sigma^z t_{nv}/2)\right], \tag{4}$$

where $\sigma^z = \pm 1$ denotes the sign of the initial projection of the reporter spin.

We have to trace over all the reporter spin projections, and, for several reporter spins, we have to add up the contributions, resulting in

$$S = \frac{1}{2}(1 + \langle \cos\phi_1 \rangle), \tag{5}$$

where $\langle\rangle$ denotes averaging over many runs of the experiment (reporter spin projections), and the phase in each run is given by the sum over all reporter spins:

$$\phi_1 = \frac{t_{nv}}{2}\sum_s k_s \sigma_s^z. \tag{6}$$

To perform this average, we use $\langle \sigma_s^z \rangle = 0$, $\langle \sigma_s^z \sigma_{s'}^z \rangle = 0$ for $s \neq s'$, $\langle (\sigma_s^z)^2 \rangle = 1$, which yields

$$S = \frac{1}{2}\left[1 + \prod_s \cos(k_s t_{nv}/2)\right]. \tag{7}$$

B. Localizing the reporter spins with DEER at several magnetic field directions

In order to map the locations of the surface reporter spins, we performed DEER experiments with varying orientation of the magnetic field, using the $\cos^2\theta$ dependence of the dipole interaction. The full Hamiltonian for the system of NV spin-reporter spin coupled via the magnetic dipole interaction is given by:

$$H = \hbar\Delta S_{z'}^2 + \hbar\gamma_e \boldsymbol{B}\cdot\boldsymbol{S} + \hbar\gamma_e \boldsymbol{B}\cdot\boldsymbol{J} + \frac{\hbar^2\gamma_e^2}{r_s^3}\left[\boldsymbol{S}\cdot\boldsymbol{J} - 3\frac{(\boldsymbol{S}\cdot\boldsymbol{r}_s)(\boldsymbol{J}\cdot\boldsymbol{r}_s)}{r_s^2}\right], \tag{8}$$

where $\Delta = 2\pi \times 2.87$ GHz is the zero-field splitting, and the z'-axis points along the NV center symmetry axis.

The zero-field splitting is the largest energy in the problem, therefore we can make the secular approximation, retaining only the terms that commute with $S_{z'}$. This amounts to fixing the direction of the vector $\boldsymbol{S}$ to be along the NV center symmetry axis. The next-largest energy term is the reporter-spin Zeeman energy $\hbar\gamma_e \boldsymbol{B}\cdot\boldsymbol{J}$. Once again we make the secular approximation, retaining only the terms that commute with $J_{z''}$, where z'' points along the direction of the magnetic field. This amounts to fixing the direction of the vector $\boldsymbol{J}$ to be along the static magnetic field. The magnetic dipole interaction can now be calculated for an abritrary magnetic field angle. We define the coordinate axes with the z-axis pointing normal to the diamond surface, and the x axis chosen so that the NV symmetry axis is in the x-z plane. Thus the unit vector along the NV axis is $(\sqrt{2}, 0, 1)/\sqrt{3}$. In order to map the location of the surface reporter spins, we perform DEER experiments for magnetic field $\boldsymbol{B}$ rotating in the x-y plane by angle ϕ, relative to the "aligned" direction. Thus the unit vector along the magnetic field is $(\sqrt{2}\cos\phi, \sqrt{2}\sin\phi, 1)/\sqrt{3}$. The vector from the NV to the reporter spin is $\boldsymbol{r} = (x, y, z)$, where z is the depth of the NV center, measured as described above.

We can now evaluate the terms in the dipole interaction Hamiltonian in eqn. (8):

$$\boldsymbol{S}\cdot\boldsymbol{J} = \frac{2\cos\phi + 1}{3} S_{z'} J_{z''}, \tag{9}$$

$$\boldsymbol{S}\cdot\boldsymbol{r}_s = \left(x\sqrt{\frac{2}{3}} + z\sqrt{\frac{1}{3}}\right) S_{z'}, \tag{10}$$

$$\boldsymbol{J}\cdot\boldsymbol{r}_s = \left(x\sqrt{\frac{2}{3}}\cos\phi + y\sqrt{\frac{2}{3}}\sin\phi + z\sqrt{\frac{1}{3}}\right) J_{z''}, \tag{11}$$

and the dipole interaction Hamiltonian:

$$H_d = \frac{\hbar^2\gamma_e^2}{r_s^3}\left[\frac{2\cos\phi + 1}{3} - \frac{\left(x\sqrt{2} + z\right)\left(x\sqrt{2}\cos\phi + y\sqrt{2}\sin\phi + z\right)}{x^2 + y^2 + z^2}\right] S_{z'} J_{z''} \tag{12}$$

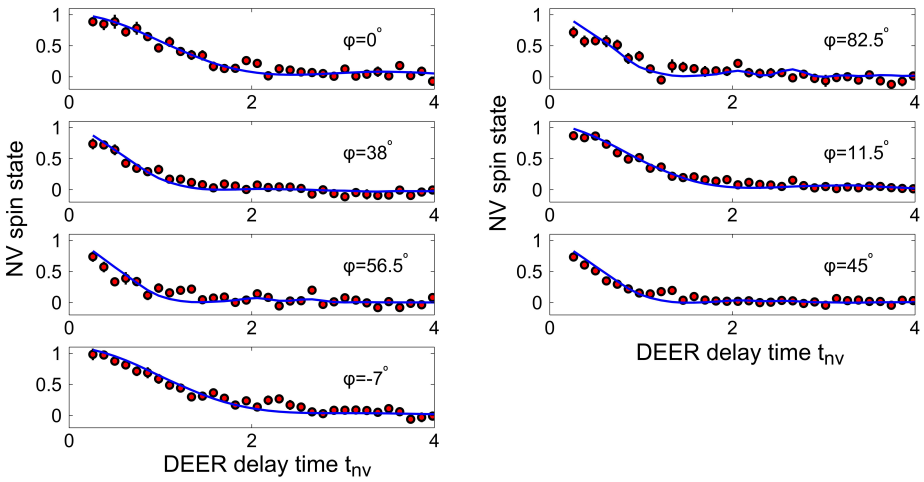

FIG. S2: DEER data taken at 7 different magnetic field angles, indicated in each plot. The magnetic field magnitude was ≈ 37 G.

Therefore, for a number of reporter spins located at positions (x_s, y_s) on the diamond surface, the NV center spin-state population after a DEER pulse sequence is given by eq. (7), with the coupling strengths

$$k_s = \frac{\hbar\gamma_e^2}{r_s^3}\left[\frac{2\cos\phi+1}{3} - \frac{\left(x_s\sqrt{2}+z\right)\left(x_s\sqrt{2}\cos\phi + y_s\sqrt{2}\sin\phi + z\right)}{x_s^2+y_s^2+z^2}\right] \tag{13}$$

The DEER experimental data at 7 different magnetic field angles ϕ are shown in Fig. S2. These data were used to produce the probability density map, shown in Fig. 1f of the main text, for the positions of 4 proximal reporter spins on the diamond surface near NV A.

C. Limits on the separation between surface reporter spins from their population relaxation

We can use the reporter-spin population relaxation measurements (Fig. 2b) to confirm that the reporter spins are well separated on the diamond surface. The rate of flip-flops between neighbor spins, due to magnetic dipole interaction, is given by[3]

$$w \approx \frac{\hbar\gamma_e^2}{4s^3}\frac{1}{4}, \tag{14}$$

where s is the separation between them, and we approximate the angular factor, that depends of the magnetic field direction, by unity. For random reporter spin positions there is likely to be a single closest neighbor that dominates the magnetic dipole interaction. If the depth of the NV center $z \lesssim s$, then the NV center interacts the strongest with a single proximal reporter spin, and the measured population relaxation time $T_1^{(s)}$ corresponds to the time scale for a single spin flip of this proximal reporter:

$$T_1^{(s)} \approx 2\pi/w \approx 32\pi\frac{s^3}{\hbar\gamma_e^2}. \tag{15}$$

If the experimentally-measured $T_1^{(s)} \approx 30$ μs is caused by the magnetic dipole interaction between surface reporter spins, then their separation is $s \approx 5$ nm. If another relaxation process limits $T_1^{(s)}$, then $s > 5$ nm.

Another possibility is $z \gg s$, so that the NV center is coupled to many reporter spins. In this case we have to consider spin diffusion, and the population relaxation time $T_1^{(s)}$, as measured by the NV center, would correspond to the time scale for spin diffusion over distance $\approx z$. This can be estimated as follows. The time scale for a single spin flip-flop is given by eq. (15), thus the time scale for diffusion over distance z is:

$$T_1^{(s)} \approx \frac{z^2}{s^2}32\pi\frac{s^3}{\hbar\gamma_e^2}. \tag{16}$$

If the experimentally-measured $T_1^{(s)} \approx 30$ μs were caused by spin diffusion in a bath of closely-spaced reporter spins, then, from eq. (16), we extract their spacing to be $s \approx 10$ nm. However, for the ≈ 3.5 nm deep NV centers that we study, this is inconsistent with the assumption $z \gg s$, and we conclude that in our experiments $z \lesssim s$, and $s \gtrsim 5$ nm, as estimated above.

IV. THE REPORTER PULSE SEQUENCE

In order to manipulate and probe the reporter spin network we use a "reporter" pulse sequence, inspired by Ramsey interferometry in atomic physics, Fig. S3. The pulse sequence is separated into two parts: the initial state readout, and the final state readout. During the initial state readout, the phase acquired by the NV center due to the surface sensor spins is ϕ_1, and during the final state readout this phase is ϕ_2. Note that these phases flip sign during the first and second halves of the NV echos, since we apply a π-pulse to the surface sensor spins simultaneously with the π-pulse on the NV. During the period between the initial and the final readout intervals, the NV acquires a phase χ, but, if we keep this time interval longer than NV T_2^*, then $\langle\chi\rangle = \langle\sin\chi\rangle = 0$, and χ does not, on average, affect the NV population. The population readout of the NV center at the end of the pulse sequence is then given by

$$S = \frac{1}{4}\left(2 + \cos(\phi_1 + \phi_2) - \cos(\phi_1 - \phi_2)\right) \tag{17}$$

$$= \frac{1}{2}\left(1 - \sin\phi_1 \sin\phi_2\right). \tag{18}$$

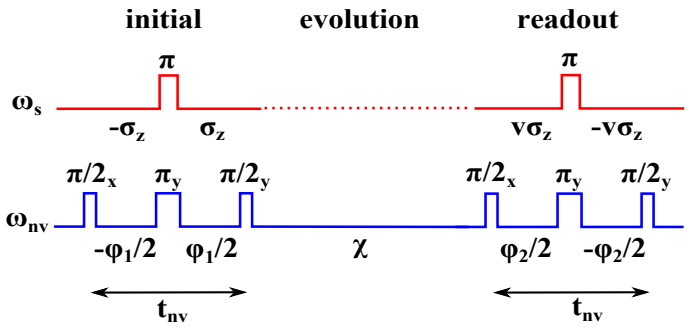

FIG. S3: Pulse sequence for NV readout of surface sensors.

Let us assume that the spin projection of a surface sensor spin s at the start of the sequence is σ_s^z, and the coupling to the NV center is k_s, as given in eq. (3). Then the NV phase ϕ_1 is given by the sum over all surface sensor spins:

$$\phi_1 = \frac{t_{nv}}{2}\sum_s k_s \sigma_s^z. \tag{19}$$

where t_{nv} is the duration of the echo.

During the surface sensor spin evolution, the projection of the surface sensor spin changes: $\sigma_s^z \to v_s^{(i)}\sigma_s^z$, where, for each run i of the experiment $v_s^{(i)} = \pm 1$ (since the spin projection can only take values $\pm 1/2$). After averaging over many experimental runs, we can average $v_s = \langle v_s^{(i)}\rangle$. For example, if we apply a π-pulse to all surface sensor spins, all $v_s^{(i)} = -1$, and $v_s = -1$. The NV phase ϕ_2 is given by

$$\phi_2 = \frac{t_{nv}}{2}\sum_s v_s^{(i)} k_s \sigma_s^z. \tag{20}$$

In this way the NV readout provides information about the surface sensor spin evolution v_s. Note that we have to average the NV population signal over all projections σ_s^z of the surface spin sensors.

We perform this average by using

$$\langle\sigma_s^z\rangle = 0,\ \langle\sigma_s^z\sigma_{s'}^z\rangle = 0 \text{ for } s \neq s',\ \langle(\sigma_s^z)^2\rangle = 1,\ v_s = \langle v_s^{(i)}\rangle, \tag{21}$$

to obtain

$$S = \frac{1}{2} - \frac{1}{4}\prod_s v_s \sin^2\frac{k_s t_{nv}}{2}. \tag{22}$$

V. SENSING NUCLEAR SPINS USING THE REPORTER ECHO SEQUENCE

A. Semiclassical spin bath

In order to measure the surface sensor coupling to proton spins, we use the pulse sequence shown in Fig. 3a, with the surface reporter spin echo. A surface reporter spin may be strongly coupled some proximal protons, and weakly coupled to many other protons that are present on the diamond surface. We describe these weakly-coupled protons as a semiclassical spin bath, whose magnetic moment precesses at the proton Larmor frequency $\omega_n = \gamma_n B$, where $\gamma_n = g_n \mu_N/\hbar$ is the nuclear gyromagnetic ratio. The magnetic moments create a fluctuating magnetic field at the location of the surface sensor spin, and the reporter spin echo modulation due to this fluctuating field is described by the factor

$$v_s(t_s) = \exp\left[-8(\gamma_n^2 B_n^2/\omega_n^2)\sin^4(\omega_n t_s/4)\right], \tag{23}$$

where B_n is the root-mean-squared amplitude of this magnetic field[4–6].

The extracted magnitude of B_n is 0.3 G, which is consistent with the magnitude of the fluctuating magnetic field created by a bath of proton spins, randomly-located on the diamond surface, with mean separation of ≈ 5.5 $\mathring{A}$. The separation between surface OH groups for a (001)-(2×1) hydroxylated diamond surface is predicted to be approximately 2.6 $\mathring{A}$[7], therefore our measurements are consistent with approximately 1/4 of the surface sites filled with protons.

B. Coherent hyperfine coupling to individual nuclear spins

The hyperfine interaction between a reporter electronic spin and a proton spin can be described by the Hamiltonian

$$H = a_0 \boldsymbol{J}\cdot\boldsymbol{I} + \frac{\hbar\gamma_e\gamma_n}{r_n^3}\left[\boldsymbol{J}\cdot\boldsymbol{I} - 3\frac{(\boldsymbol{J}\cdot\boldsymbol{r}_n)(\boldsymbol{I}\cdot\boldsymbol{r}_n)}{r_n^2}\right], \tag{24}$$

where $\boldsymbol{J}$ is the spin operator of the reporter qubit, $\boldsymbol{I}$ is the proton spin operator, r_n is the separation between the surface sensor spin and the nuclear spin, and a_0 is the contact hyperfine interaction. In the secular approximation the oscillating terms with J_x and J_y can be neglected, and the Hamiltonian reduces to $H = \hbar a J_z I_z + \hbar b J_z I_x$, where

$$a = a_0 + \frac{\hbar\gamma_e\gamma_n}{r_n^3}\left(1 - 3\cos^2\theta_n\right), \tag{25}$$

$$b = \frac{\hbar\gamma_e\gamma_n}{r_n^3}\left(3\cos\theta_n \sin\theta_n\right), \tag{26}$$

where θ_n is the angle between the vector between them and the applied magnetic field B. The spin projection of the reporter spin s, coupled to a nuclear spin n, after the echo sequence is described by the expression[8]:

$$v_{s,n}(t_s) = 1 - 2\left(\frac{b\omega_n}{\omega^+\omega^-}\right)\sin^2(\omega^+ t_s/4)\sin^2(\omega^- t_s/4), \tag{27}$$

where

$$\omega^{\pm} = \sqrt{(\pm a/2 - \omega_n)^2 + b^2/4}. \tag{28}$$

If the surface sensor is coupled to several proximal nuclear spins, as well as the weakly-coupled nuclear spin bath, then

$$v_s(t_s) = \exp\left[-8(\gamma_n^2 B_n^2/\omega_n^2)\sin^4(\omega_n t_s/4)\right]\prod_n v_{s,n}(t_s). \tag{29}$$

C. Fitting experimental data

In addition to the interaction with nuclear spins, the reporter spin decoherence rate Γ_s is a fitting parameter. The final expression used for fitting surface spin sensor echo modulation is:

$$v_s(t_s) = e^{-\Gamma_s t_s} \exp\left[-8(\gamma_n^2 B_n^2/\omega_n^2)\sin^4(\omega_n t_s/4)\right] \prod_n v_{s,n}(t_s), \tag{30}$$

where the product is over the strongly-coupled nuclear spins.

Finally, if the NV center is coupled to several surface sensor spins,

$$S = \frac{1}{2} - \frac{1}{4}\prod_s v_s \sin^2 \frac{k_s t_{nv}}{2}, \tag{31}$$

as in eq. (22).

The fits shown in Fig. 4a and 4b were performed by first using the DEER data to extract the magnetic dipole coupling constant k_s of the NV center to the proximal reporter spin, and fitting the reporter spin echo data using eqn. (30), with one or two coherently-coupled protons, and a proton spin bath, see Table I for relevant best-fit parameters for the fits shown Fig. 3a and Fig. 4a,b of main text.

In order to calibrate the reporter spin state, we performed two measurements using the reporter sequence: (i) with no pulse in the evolution segment, and (ii) with a π-pulse in the evolution segment. These were taken to correspond to (i) no reporter spin state change $\rightarrow +1$, and (ii) reporter spin flip $\rightarrow -1$. The reporter sequence measurements in this work were done in pairs, with the reporter evolution sequences differing by a reporter π-pulse. For example, the reporter echo measurement was done first with the reporter pulses $\pi/2$-π-$\pi/2$, immediately followed by a sequence $\pi/2$-π-$3\pi/2$. We confirmed that these measurements resulted in opposite final reporter spin populations.

NV center	magnetic field	parameter	best-fit value
NV A	383 G	k_s	1.6 μs^{-1}
		Γ_s	1.3 μs^{-1}
		ω_n	10.6 μs^{-1}
		reduced χ^2	1.2
NV A	619 G	k_s	1.6 μs^{-1}
		Γ_s	1.8 μs^{-1}
		ω_n	19 μs^{-1}
		reduced χ^2	1.3
NV B	665 G	k_s	1.4 μs^{-1}
		Γ_s	1.3 μs^{-1}
		ω_n	17.1 μs^{-1}
		reduced χ^2	1.1

TABLE I: Best-fit parameters.

VI. CONTROL EXPERIMENT: ACID-CLEANING THE DIAMOND SURFACE

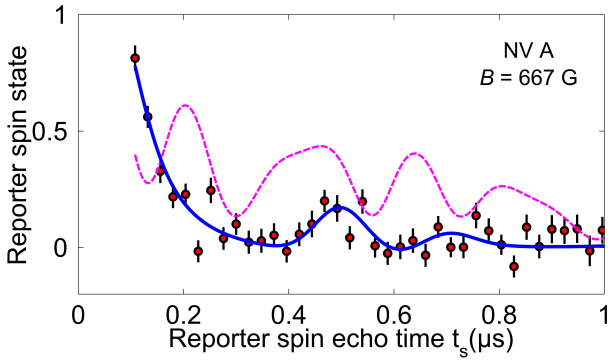

FIG. S4: The NV A reporter spin echo measurement after 3-acid surface treatment. The best-fit curve for the measurement before the surface treatment is shown as a dashed magenta line (see also Fig. 4a of main text).

Treatment of the diamond crystal surface with the strongly-oxidizing 3-acid mixture (equal volumes of concentrated H_2SO_4, HNO_3, and $HClO_4$) for two hours re-sets the locations of the surface reporter qubits (Fig. 1e of main text). We also repeated the reporter spin echo experiment on NV A after this surface treatment, see Fig. S4. The data are clearly modified, indicating that this measurement is sensitive to the interaction between the reporter spin at a new, post-clean, location, with protons in its vicinity on the diamond surface.

* Hongkun_Park@harvard.edu
† lukin@physics.harvard.edu

[1] L. M. Pham, S. J. DeVience, I. Casola, Francesco Lovchinsky, A. O. Sushkov, E. Bersin, J. Lee, P. Cappellaro, H. Park, A. Yacoby, M. Lukin, and R. L. Walsworth, manuscript in preparation.
[2] Y. Chu, N. P. de Leon, B. J. Shields, B. Hausmann, R. Evans, E. Togan, M. J. Burek, M. Markham, A. Stacey, A. S. Zibrov, A. Yacoby, D. J. Twitchen, M. Loncar, H. Park, P. Maletinsky, and M. D. Lukin, Nano letters **14**, 1982 (2014).
[3] A. Abragam, *The principles of nuclear magnetism* (1961).
[4] L. Childress, M. V. Gurudev Dutt, J. M. Taylor, A. S. Zibrov, F. Jelezko, J. Wrachtrup, P. R. Hemmer, and M. D. Lukin, Science **314**, 281 (2006).
[5] H. J. Mamin, M. Kim, M. H. Sherwood, C. T. Rettner, K. Ohno, D. D. Awschalom, and D. Rugar, Science **339**, 557 (2013).
[6] T. Staudacher, F. Shi, S. Pezzagna, J. Meijer, J. Du, C. A. Meriles, F. Reinhard, and J. Wrachtrup, Science **339**, 561 (2013).
[7] S. Sque, R. Jones, and P. Briddon, Physical Review B **73**, 085313 (2006).
[8] L. Rowan, E. Hahn, and W. Mims, Physical Review **137**, A61 (1965).